Applied Mathematical Modelling 40 (2016) 10404–10418

Contents lists available at ScienceDirect

Applied Mathematical Modelling

journal homepage: www.elsevier.com/locate/apm

Large eddy simulation of surge inception and active surge control in a high speed centrifugal compressor with a vaned diffuser

Ibrahim Shahin[a,b,*], Mohamed Alqaradawi[a], Mohamed Gadala[c], Osama Badr[d]

[a] Mechanical and Industrial Engineering Department, College of Engineering, Qatar University, Doha 2713, Qatar
[b] Mechanical Engineering Department, Shoubra Faculty of Engineering, Benha University, Egypt
[c] Mechanical Engineering Department, UBC-University of British Columbia, Vancouver, BC, Canada
[d] Mechanical Engineering Department, the French University in Egypt, Al-Shorouk City, New Cairo, Egypt

ARTICLE INFO

Article history:
Received 31 August 2014
Revised 28 June 2016
Accepted 21 July 2016
Available online 28 July 2016

Keywords:
Active surge control
Aero engine
Centrifugal compressor
Self-recirculating bleed slots location

ABSTRACT

In this study, we present a numerical investigation of active surge control and performance improvement for an aero engine centrifugal compressor (NASA CC3) using self-recirculating bleed slots with different bleeding positions. This investigation considers an unsteady three-dimensional numerical simulation based on large eddy simulation. Three bleeding slots positions are studied and compared with a compressor without surge control. The aim of the recirculating bleed slots is to remove some of the reversed flow during surge inception from the impeller inducer, which influences the stable operating range and compressor pressure ratio. The effects of the three bleeding slot positions on the internal flow and performance of the compressor are highlighted by a detailed analysis of the impeller flow field. The surge event stages are detected well inside the impeller and diffuser. The results show that an effective flow bleeding system can increase the surge limit compared with a classical compressor without a bleeding system. A comparison of the cases investigated in this study indicates that the surge limit increases by 8% for the bleeding slots located closer to the main blade leading edge, with lower increase in the surge limit for slots near the split blade's leading edge.

1. Introduction

Engineering applications may require a centrifugal compressor with a wide and safe operating range, especially for power generation, in the natural gas industry, and aero propulsion. Thus, extending the operating range of compressors has been the focus of many previous studies. The safe operating range for a centrifugal compressor is limited by the choke and surge point. A centrifugal compressor in a surge and stalled condition will have an unstable internal flow and unfavorable system operation. During the compressor surge, the rotating impeller and stationary parts experience large pressure transients, high loads, and high temperatures, which can result in extensive damage to the internal parts in some cases.

Abbreviations: CFD, computational fluid dynamics; LES, large eddy simulation; NASA, National Aeronautics and Space Administration; LE, Leading Edge; URANS, Unsteady Reynolds Averaged Navier Stokes.

* Corresponding author.
E-mail addresses: Ibrahimshahin@qu.edu.qa, Ibrahim.shahin@feng.bu.edu.eg (I. Shahin), myq@qu.edu.qa (M. Alqaradawi), gadala@mech.ubc.ca (M. Gadala), Osamaabadr@outlook.com (O. Badr).

http://dx.doi.org/10.1016/j.apm.2016.07.030
0307-904X/

Nomenclature

U_2	impeller tip speed (m/s)
R	radius (mm)
ρ	fluid density (kg/m^3)
u	flow velocity vector
u_g	mesh velocity of the moving mesh (m/s)
T	diffusion coefficient
ϕ	source term of ϕ

1.1. Rotating stall and surge

Many experimental studies have been performed to explore rotating stall and surge phenomena in centrifugal compressors. During the last decade, many researchers have investigated stall and surge in transonic compressors to understand the internal flow pattern during stable and unstable operation. The detailed design of the NASA CC3 centrifugal compressor was presented by Mckain and Holbrook [1], where the geometrical parameters were defined for a single stage compressor with a pressure ratio equal to 4. Experimental and numerical studies have investigated surge onset in the NASA CC3 centrifugal compressor. In particular, Spakovszky [2] showed that the unsteady blade-row interaction and coupling is driven by the resonant behavior of the rotor and the stator wave systems. In addition, the existence of backward travelling stall precursors was shown, which was confirmed experimentally and numerically by Skoch et al. [3] and Wernet et al. [4], respectively. Ni and Fan [5] numerically studied the NASA CC3 compressor to generate a compressor performance map. The numerical results were validated with experimental results, which determined the internal flow structure and helped to improve the compressor's performance. Lurie et al. [6] performed a numerical analysis of the unsteady impeller–diffuser interaction for a high-efficiency, compact centrifugal compressor stage. Their results showed that the final total-to-static adiabatic efficiency of the compressor increased by 1.7% and the stage's maximum diameter decreased by 23%.

Lim et al. [7] employed a test rig to investigate surge phenomena and surge control for a centrifugal compressor, where the active magnetic bearings servo actuation method was used to control the impeller tip clearance. Trébinjac et al. [8] performed numerical and experimental investigations of a vaned diffuser centrifugal compressor, where the numerical simulation was performed using the Elsa code [8]. They studied the effect of changing the operating point from choke to surge on the internal flow structure. An internal recirculation method was described by Babak [9] as a surge suppression device in order to increase the stable operating range for a centrifugal compressor. Galindo et al. [10] studied the effects of the amplitude and frequency of pressure pulses on the surge margin of a compressor. Numerical and experimental investigations of a transonic centrifugal compressor were reported by Bulot et al. [11], who studied the flow inside the impeller when the compressor operated near the surge condition. Bulot and Trébinjac [12] investigated the flow inside the vaned diffuser of a transonic high-pressure centrifugal compressor stage, where they performed three-dimensional, time-dependent, unsteady computations of the stage using a three-dimensional Navier–Stokes code with a phase-lagged technique. They only conducted their investigations at the operating point close to the design point.

Numerical and experimental studies were conducted by Arnulfi et al. [13] based on a compression system in the surge condition, where different surge control devices were tested and compared. Stein [14] developed a new numerical method to simulate the transient viscous fluid flow in turbo-machinery parts and this method was used to investigate the phenomena that cause flow instabilities in a centrifugal compressor. The results showed that at lower flow rates, large flow incidence angles can lead to flow separation at the blade's leading edge. Ferrara et al. [15] experimentally investigated the influence of vaneless diffuser types on stall behavior, where different widths, pinch shapes, and diffusion ratios were tested. Their results indicated that the diffusion ratio has a large effect on the stall pattern and on the stall onset operating point. Gravdahla et al. [16] presented a new method for active surge control in a centrifugal compressor. Their results showed that the stable operating range of the centrifugal compressor can be extended by using the rotational speed of the motor for control.

1.2. Surge control

Many studies have aimed to increase the stable operating range of a centrifugal compressor, where the use of self-recirculating bleeding slots is one of the most common and efficient active methods for increasing the surge margin of a centrifugal compressor. Recently, Sivagnanasundaram et al. [17] reported an experimental and steady state numerical investigation where they used guide vanes in the annular cavity of bleeding slots. The guide vanes were designed to reduce the swirl that could develop in the bleed slot. In an experimental and computational study, Beneda [18] investigated the effect of a variable inducer shroud bleed and blade load distribution control on the compressor surge limits and efficiency. These two methods can be developed and utilized as active surge suppression units with increased efficiency. Hu et al. [19] numerically and experimentally studied the effects of using active self-recirculation, where the results indicated that the choke limit can be increased by 15% and the surge limit by 20% with no effect on the compressor efficiency. Yamaguchi [20] indicated that the use of a cavity with guide vanes increased the compressor map width by 20% compared with a bleed slots

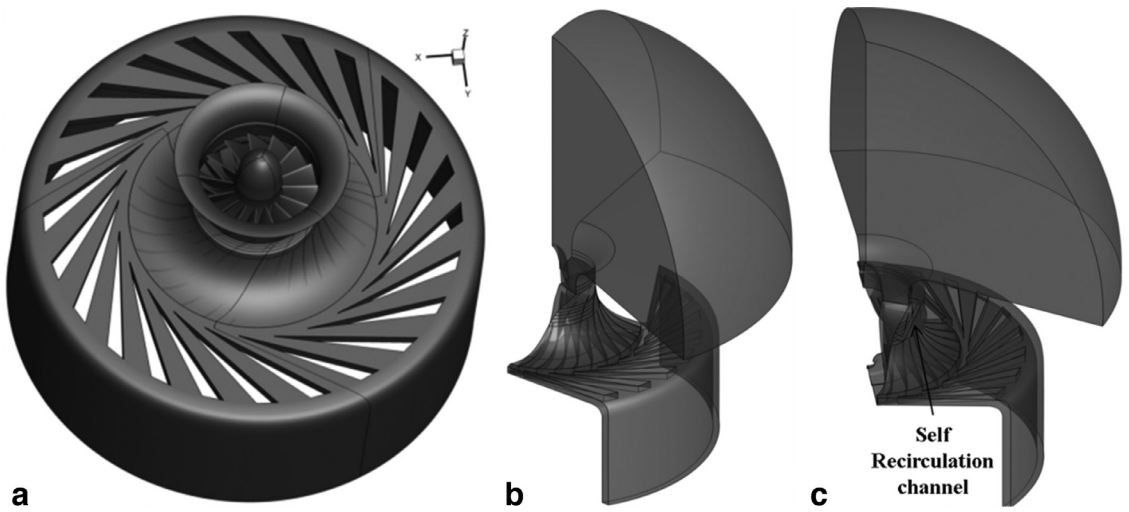

Fig. 1. Geometry considered in this study: (a) base case computational domain, and (b) bleeding slots computational domain.

system without guide vanes. The guide vanes caused a counter swirl at the inducer inlet with an appropriate vane design. Tamaki et al. [21] discussed the characteristics of turbochargers with and without self-recirculation slots, and the effects of using axisymmetric bleed slots were also studied for a compressor with a high pressure ratio. Experiments demonstrated the effects of two nonaxisymmetric recirculation slots on the compressor's performance, where the results showed that one bleed slot had a sine wave pattern and the other bleed slot was partially channeled in the circumferential direction.

Tamaki [22] conducted a numerical study to increase the stable operating range of a centrifugal compressor. Steady state three-dimensional calculations were performed to investigate two different types of recirculation slots: conventional slots with no guide vanes and new recirculation slots with vanes installed in the cavity. The results indicated that the vanes gave the recirculation flow a negative pre-swirl at the inlet of the impeller in the direction counter to the impeller rotation. Experimental and numerical studies of the interaction between the recirculation device and the compressor impeller flow were conducted by Dickmann et al. [23], where the effects of the intake elbow and volute casing were also studied. Many active surge control techniques have been reported previously [24–26]. Mingyang et al. [27] investigated the unsteady effects of recirculation slots on the internal flow in a centrifugal compressor based on numerical and experimental studies. Their results indicated that recirculation slots can damp the distortion that propagates from downstream, thereby reducing the flow distortion at the inlet. Furthermore, the width of the rear slot had a large effect on reducing the flow distortion. Numerical calculations showed that the fluctuations in the re-circulated flow rate due to the front slot were damped by the recirculating slots.

However, a review of previous studies of active surge control methods indicates that aero engine centrifugal compressors have received less attention than small turbo charging compressors. By contrast, the interference generated in turbo charging compressors has been considered often due to the high production level and its wider applications in the diesel-engine industry. The brief review given above also indicates the common shortcomings of previous studies. In particular, most were computational studies (except for [23] and [27]) using a steady frozen rotor model, thereby neglecting the unsteadiness and the interaction between the vanes used in the cavity and inducer blades. In addition, a self-recirculating casing treatment was used only for the turbocharger compressor and it has not been investigated for an aero-propulsion compressor. Thus, the flow field data obtained in the preset study can be used to optimize the locations of bleed slots for the active control of rotating stall and surge. Previously, we numerically studied the development of stall and surge phenomena in a transonic centrifugal compressor [28–30]. The unsteady flow structure and blade loading during the surge condition were analyzed without using any active surge control methods. In the present study, we use the active recirculation bleeding slots to increase the surge margin of a centrifugal compressor used in aero engines. The effects of the bleed slot port positions are also investigated based on large eddy simulations (LESs).

2. NASA CC3 compressor

A NASA CC3 compressor was studied experimentally at the Small Engine Components Test Facility at NASA Glenn Research Center [2-4] and Fig. 1a shows the geometry of the NASA CC3 compressor. The numerical model is divided into stationary and rotating parts: the inlet spherical domain with an inlet bell at its end, the impeller rotating domain, a stationary vaned diffuser, and the back hub cavity of the impeller followed by a shaft seal. The dimensions of the rotating and stationary parts are shown in Table 1. The design operating conditions are summarized in Table 2. The impeller outflow is directed to a wedged vaned diffuser followed by an annular radial-to-axial bend. The exit axial part length is increased more than the actual case to avoid the effect of the pressure outlet boundary condition on the calculations inside the

Table 1
Impeller and diffuser dimensions.

Dimension	Impeller
No. of main blades	15
No. of splitter blades	15
Back sweep angle	50°
Inlet diameter D_1	210 mm
Outlet diameter D_2	431mm
Inlet blade height	64 mm
Exit blade height	17 mm
Tip clearance at Leading Edge	0.154 mm
Tip clearance at mid-chord	0.61 mm
Tip clearance at exit	0.203 mm
Dimension	**Vaned diffuser**
No. of diffuser vanes	24
Diffuser vane's leading edge	108%R_2
Diffuser divergence angle	7.8°
Diffuser area ratio	2.75
Inlet diameter	431 mm
Outlet diameter	714 mm
Vane height	17 mm

Table 2
Operating and unsteady simulation parameters.

Condition	Value
Designed inlet pressure bar	1.013
Designed pressure ratio	4:1
Inlet temperature (K)	288
Design mass flow rate (lbm/s)	10
Surge mass flow rate (lbm/s)	9.3916
Rotational speed (rpm)	21,789
Total simulated flow time (s)	0.122
Time step (s)	6.6e−6
Number of time steps	18,485
Number of iterations per time step	10
Hardware operating time per case day	90

diffuser domain. Fig. 1b shows the base case geometry used to simulate the impeller and diffuser parts. In order to reduce the calculation time, only a 120° sector is simulated, including five impeller main/splitter blade pairs and eight vanes from the diffuser. Fig. 1c shows the conditions with self-recirculating casing treatment. Recirculating bleed slots are used to remove some of the reversed flow during surge inception from the impeller inducer, where three bleeding slots positions are studied, as shown in Fig. 2. The bleeding position is changed relative to the main blade leading edge, whereas the reinjection slot position is fixed in the three cases considered.

3. Numerical method

3.1. Model setup

The unsteady compressible Navier–Stokes equations [1] are solved. The moving sliding mesh method is used to simulate the impeller rotation. In this method, the stationary and moving cell zones are connected with each other by using the interface boundary conditions. When the mesh motion is updated in time, the non-conformal interfaces are also updated to reflect the new positions of each zone [17]. The general integral form of the conservation equation formulation for a general scalar, ϕ, on an arbitrary control volume, V, with a moving boundary, can be written as follows.

$$\frac{d}{dt}\int_V \rho\phi dV + \int_{\partial V} \rho\phi(\vec{u}-\vec{u}_g)\cdot d\vec{A} = \int_{\partial V} \vartheta\nabla\phi\cdot d\vec{A} + \int_V S_\phi dV. \tag{1}$$

Unsteady large-scale structures and separation zones are the main characteristics of the flow in the centrifugal compressor, so the LES approach is employed. In LES, large eddies are resolved directly, whereas small eddies are modeled with a subgrid scale model. A major role of the small scales is to dissipate the turbulent energy transferred from the larger scales to the smaller scales via the energy cascade. In the LES approach, separation between the resolved and unresolved scales is achieved by low-pass spatial filtering of the governing equations. The subgrid-scale stresses resulting from the filtering operation are unknown, and thus they must be modeled. In the present study, we use the subgrid Smagorinsky–Lilly model

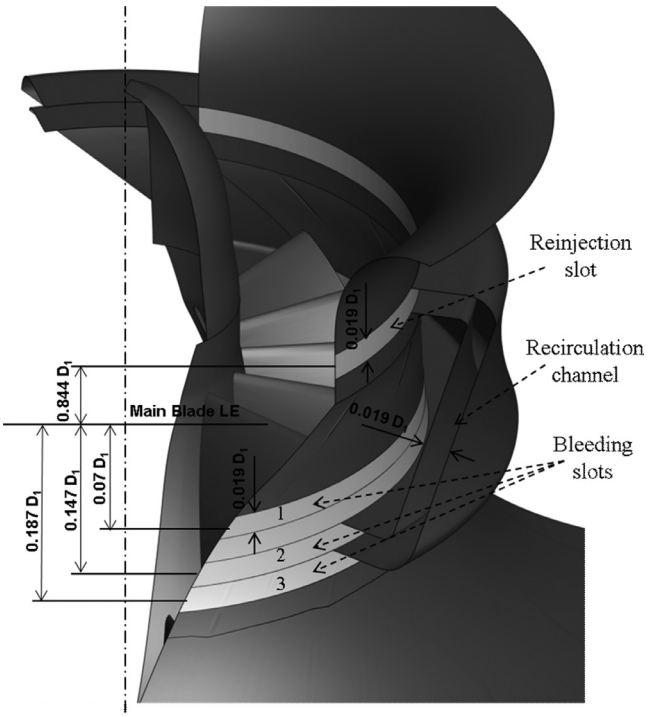

Fig. 2. Bleeding slots drawing and dimensions.

and the eddy viscosity is modeled by:

$$\mu_t = \rho L_s^2 \sqrt{2\bar{S}_{ij}\bar{S}_{ij}},$$

where LS is the mixing length for the subgrid scales, which is the rate of the strain tensor for the resolved scales:

$$L_s = min(\kappa d, C_s \Delta),$$

where κ is the von Karman constant, d is the distance to the closest wall, C_s is the Smagorinsky constant, and Δ is the local grid scale. In the present study, Δ is computed according to the volume of the computational cell using the following equation.

$$\Delta = V^{1/3}.$$

The second order accuracy is used as a discretization method in space and the moving sliding mesh is used to simulate the impeller's rotation. The relative position at the interface between the moving impeller and stationary parts is updated over time.

3.2. Mesh generation and boundary conditions

ICEM computational fluid dynamics (CFD) was used to generate the structured grid for the compressor with no bleeding slots and the compressor with different bleeding slot positions. Hexahedral elements were used to mesh the computational domain with about 9,629,414 cells for the simulated 120° sector, as shown in Fig. 3. The grid was refined at the compressor walls to capture the boundary layer. In order to accurately predict the tip flow, 10 cells were used in the tip clearance between the blade tip and compressor casing. The grid was refined close to the wall in order to capture near-wall effects, where the distance to the first grid point from the wall was set such that the viscous wall distance ($y+$) was near 1. The mass flow was specified at the inlet of the compressor and the inlet air pressure was set at atmospheric pressure and 288 K. Interface boundary conditions were used at the interface between each rotating and stationary part, pressure outlet boundary conditions were used at the domain outlet, a rotating periodic boundary condition was used, and wall boundary conditions with no slip velocity were employed on the walls. The CFD code FLUENT with parallel processing version 14.5 [31] was used to solve the filtered governing equations, which were discretized by the finite volume method. A second-order upwind scheme was used for spatial discretization. The second-order implicit formulation was used for temporal discretization. In order to resolve the relevant fluctuations, the grid resolution must be high with a small time step and the Courant number should be smaller than unity to be consistent with the flow properties, so in this study, we used a time step of 6.119e−6.

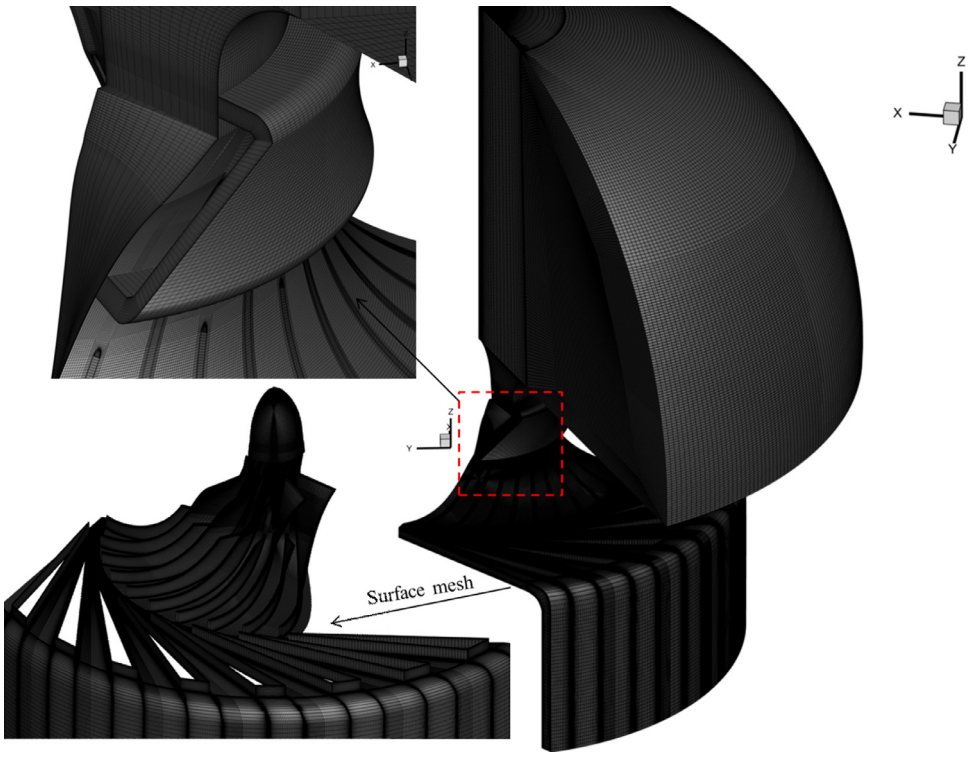

Fig. 3. Details of the computational domain mesh.

Table 3
Performance parameters under the designed flow rate with different numbers of computational nodes.

No. of computational nodes	Pressure ratio		Overall efficiency	
	Experimental Skotch et al. [3]	Present CFD	Experimental Skotch et al. [3]	Present CFD
6,830,000	4.1	3.72	0.84	0.87
9,630,000		4.17		0.85
13,270,000		4.195		0.846

The sliding mesh method was used to simulate the impeller's rotation, which requires more time for calculations than other methods such as moving reference frame. The sliding mesh simulated the impeller rotation as found in the actual system, which captured the relative positions of the impeller and the stationary parts well. The rotator stator interaction was captured and the relevant fluctuations were resolved during the simulation period. The numerical calculations were performed by high-performance parallel computing using a DELL server with four AMD Opteron processors, 48 cores, and 128 GB of RAM. In order to assess the convergence of the solution, the residual levels and flow properties were monitored during the calculations. The residual levels were examined and relevant integrated quantities such as the pressure and mass flow were also monitored during the iterations. The data monitor and residual levels of "1e−4" were used to assess the computational convergence of the unsteady calculations. The imbalance (or error) of the residuals in conservation equations is usually measured and scaled relative to the local value of the property in order to obtain the relative error. The mass flows at the duct inlet, impeller inlet, impeller outlet, and diffuser outlet were monitored during the calculations, while the static and dynamic pressure were monitored at different locations in the simulation domain, such as the impeller inlet, impeller outlet, and diffuser outlet.

3.3. Mesh sensitivity study

To ensure the reliability of the numerical model, we carefully checked for grid independence using three computational node sizes: 6.83, 9.63, and 13.27 million nodes. The number of nodes was changed by increasing the number of elements for the impeller and diffuser in the meridional, radial, and spanwise directions. The performance parameters for the design flow rate in the three tested computational meshes are shown in Table 3, according to the experimental results reported by Skotch et al. [3] and the present CFD. Clearly, the CFD results obtained with 9.63 million computational nodes agreed

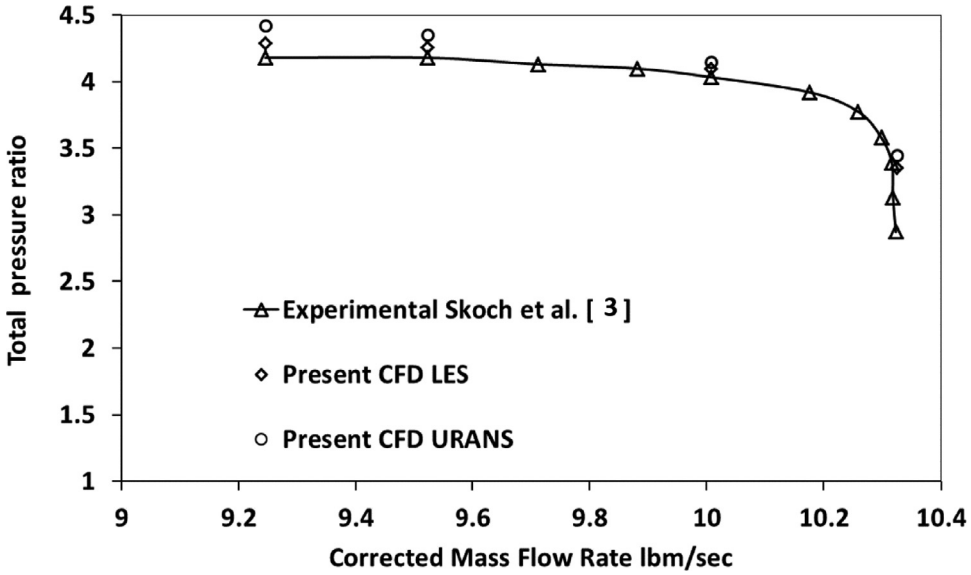

Fig. 4. Pressure ratio of the compressor stage for the CFD results obtained by the URANS and LES models, and previously reported experimental results [3].

Table 4
URANS simulation parameters.

Condition	Value
Turbulence model	RNG-K-ε
Model constants	$C_{mu} = 0.09$ $C_{1-\varepsilon} = 1.44$ $C_{2-\varepsilon} = 1.92$
Near-wall treatment	Non-equilibrium wall function
Turbulence intensity at inlet	5%
Time step	6.6e−6
Number of iterations per time step	20

well with the experimental data [11], and there were no noticeable changes after increasing the number of nodes to 13.27 million nodes. Thus, the grid with 9.63 million nodes was used in all of the simulations.

3.4. Numerical model validation

In this section, we compare the numerical model results with previously reported experimental results [11] to ensure the accuracy and reliability of the model. The total pressure ratio of the compressor is shown in Fig. 4 for the numerical model based on URANS and LES, which is compared with the experimental results obtained by Skotch et al. [3]. The URANS parameters are shown in Table 4. The trend in the experimental results was predicted well by the URANS approach, but the pressure ratio was overestimated at off-design operating points, especially near the stall limit. Under the designed operating conditions, URANS slightly overestimated the pressure ratio whereas the results based on LES were in good agreement with the experimental results at the design operating point and lower flow rates. In order to validate the unsteady flow variations, the instantaneous velocity contours at 95% of the span plan for the diffuser throat are shown in Fig. 7. We compared our CFD results with the measurements obtained by Wernet et al. [4] at different time instances during the surge cycle. Fig. 5a shows the normal flow conditions immediately before the surge's onset, where the CFD predicted the distribution correctly compared with the measurements because the maximum velocity was 375 m/s at the minimum area and the velocity decreased gradually toward the diffuser exit in the range between 125 m/s and 150 m/s. The reverse flow phase of the surge cycle is shown in Fig. 5b, where the numerical results predicted the appearance of a back flow with a maximum velocity value around 110 m/s at the diffuser throat, and this result was similar to the experimental result of 112 m/s. The peak velocity in the diffuser condition corresponding to the minimum pressure was also predicted well, as shown in Fig. 5c, where a small region with a corrected flow direction appeared at the diffuser throat, and the numerical results were the same but with slightly higher velocity magnitudes. According to Fig. 5, we may conclude that our CFD model with LES could accurately capture the complex unsteady flow variations during the surge.

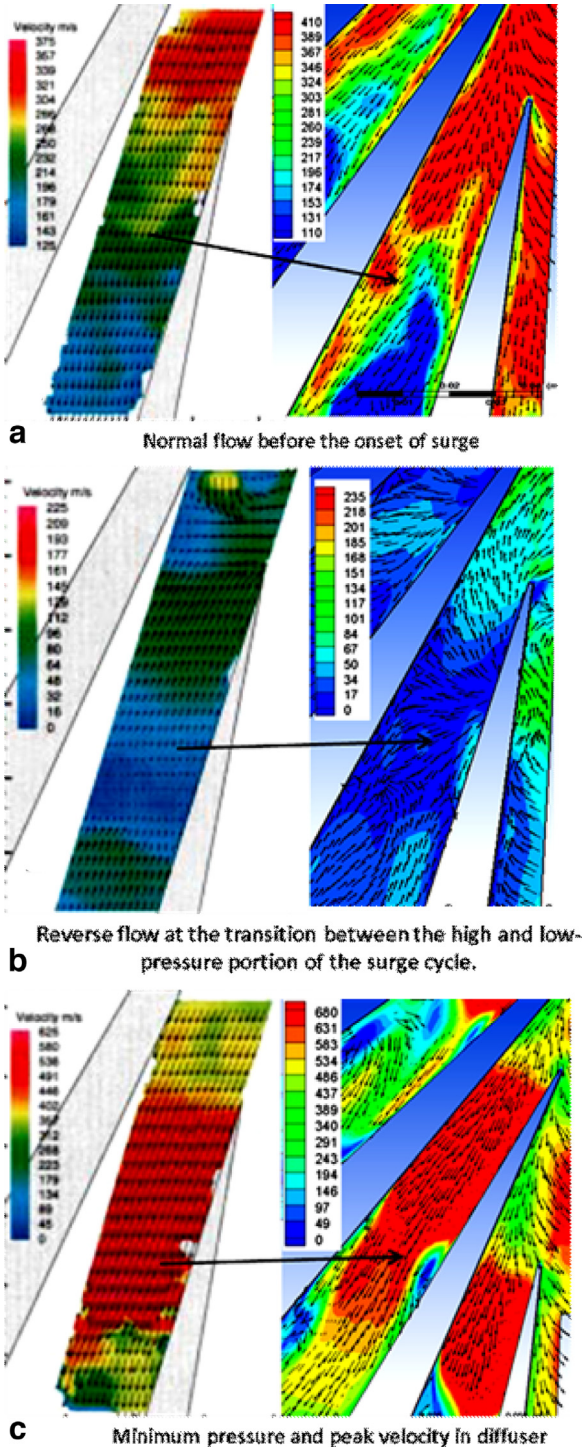

Fig. 5. Comparison of the measured velocities [4] (left) and simulation of the vaned diffuser under different flow conditions during the surge event (right).

4. Surge inception characteristics

We investigated the unsteady flow pattern in the surge condition by recording the area-weighted average static pressure and mass flow rate during the simulation period at several locations. All of the monitored signals were obtained when the operating point moved immediately after the surge limit at a mass flow of approximately 4.26 kg/s and 21,789 rpm. Fig. 6

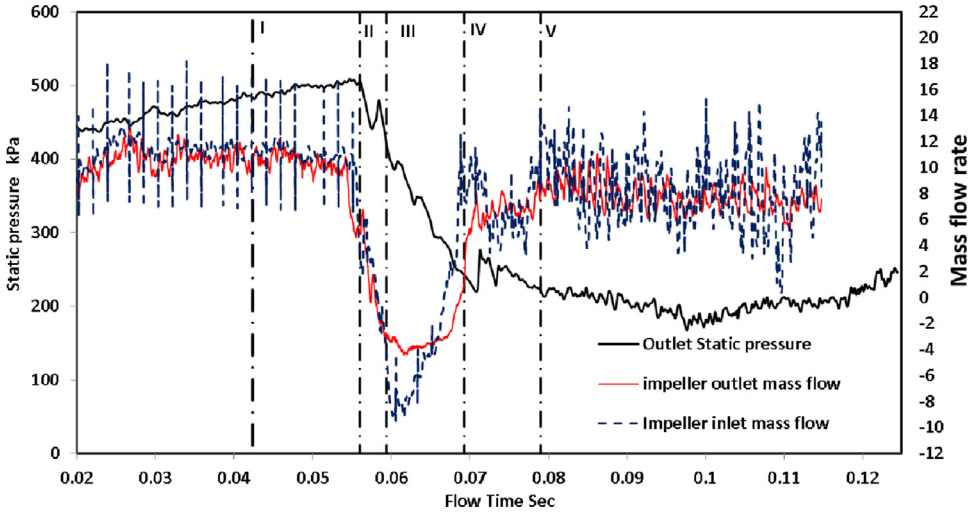

Fig. 6. Area-weighted average of the instantaneous static pressure in the diffuser outlet plane and the mass flow rate in the impeller with the flow time.

shows the time-resolved mass flow rate at the diffuser exit, which indicates that the fluctuations in the outlet mass flow had noticeably higher amplitude fluctuations and the amplitude reached the maximum value during the period when the backflow occurred. The instantaneous static pressure at the diffuser outlet is also shown in Fig. 6. The model predicted the deep surge development well when the mass flow decreased below the surge limit. The instantaneous outlet static pressure increased with time until a value at which the impeller could not overcome the back pressure at the diffuser. In this condition, the fluid with a high pressure in the vaned diffuser area returned back into the vaneless diffuser area, which caused a sudden decrease in the diffuser pressure. The pressure in the diffuser area started to increase again from the lowest value back to the stable operating point pressure level before the next surge cycle commenced. The impeller flow during the surge was characterized by even larger mass flow oscillations, which became negative in part of the cycle, as shown in Fig. 6. Under the reverse flow, the instantaneous operating point moved down a line known as the negative flow characteristic. The impeller inlet was subject to high fluctuations in the flow rate during the surge and the flow also reversed at the impeller front. The surge onset event was marked by the high amplitude of the pressure, which started to increase with a distinct fluctuation frequency and it reached a maximum value of 510 kPa, as measured by Wernet et al. [4], which is indicated in Fig. 6.

5. Descriptions of the surge stages

(i) **Pre-surge interval:** This phase started when the mass flow decreased to the surge flow, which caused an increase in the back pressure and flow, where they separated on the diffuser vane walls. As shown in Fig. 7, rotating instabilities were observed in the passage toward the diffuser exit. In addition, there was a larger area with low-momentum fluid on the suction side of the diffuser channels. The low-momentum fluid on the diffuser channels caused a reduction in the effective flow area. Before the initiation of the surge event, a corner-separated flow developed near the hub corner immediately after the vane's leading edge.

(ii) **Surge inception:** This phase was caused by the large increase in the static pressure in the diffuser channels. Rotating instabilities were a major characteristic of this phase. A number of stall cells were observed near the diffuser vane's trailing edge. The fluctuations in the mass flow rate and the pressure caused an increase in the rotating stall cell's size, and thus a larger blockage developed in the diffuser channels. The impeller developed pressure to move the fluid against the blockage in the diffuser, which caused the surge event. Fig. 7 shows the changes in the flow features of the diffuser during the surge intervals. A stall zone appeared toward the pressure side on part of the diffuser vane passage, which built up and then died down. Weak recirculation was detected in some passages close to the vane's pressure side. By contrast, a similar but much stronger recirculation was detected in other passages, which was closer to the center and suction side, as also observed by Wernet et al. [12].

(iii) **Flow reversal interval:** The low-momentum fluid and stalled zones in the diffuser caused a decrease in the flow area of the diffuser, thereby increasing the pressure until the impeller developed a pressure that could no longer overcome the adverse pressure from the diffuser passages. The higher pressure fluid in the compressor exit area moved backward into the impeller exit, which resulted in a pressure failure (Fig. 6). A back flow through the diffuser channels was observed during this interval (Fig. 7–III), where the relative positions of the impeller blades and the diffuser vane affected the characteristics of the reversing flow. Some passages of the diffuser had a completely reversed flow

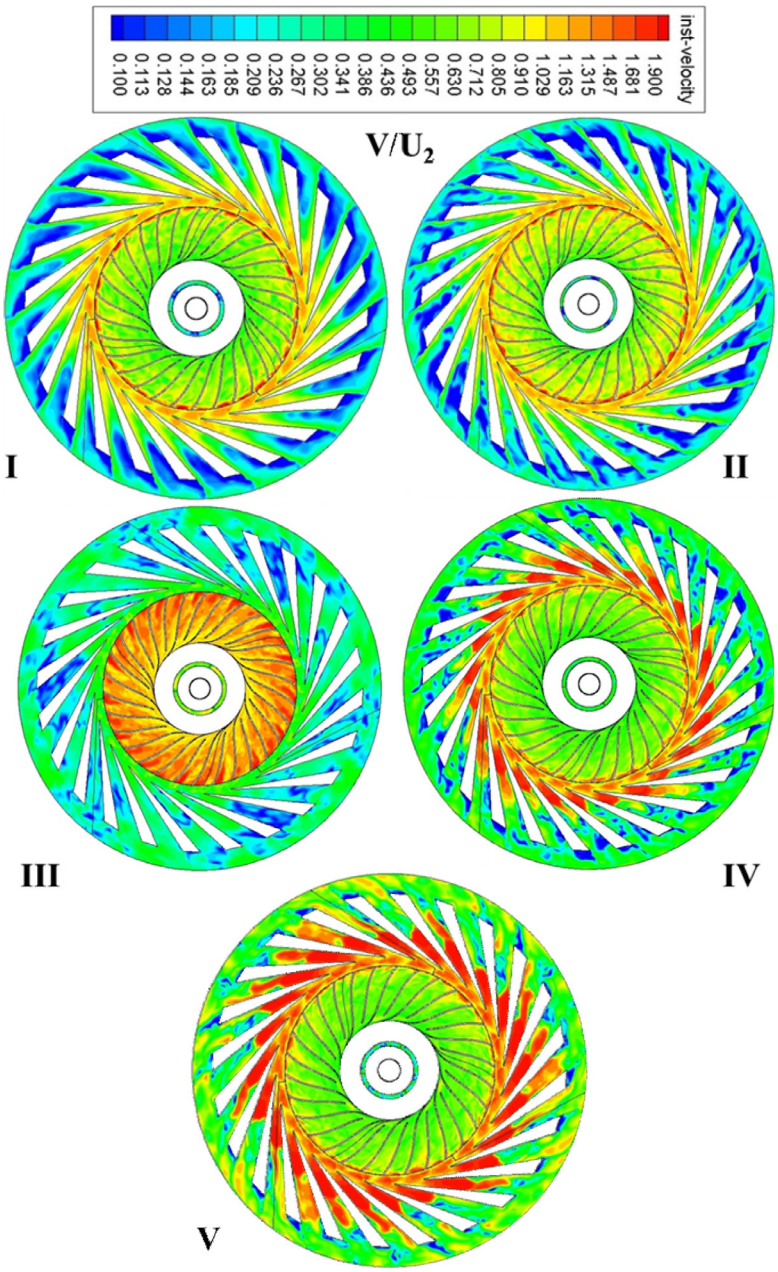

Fig. 7. Dimensionless instantaneous velocity "V/U_2" at 95% of the span plane during the surge stages.

during the backflow, whereas others exhibited flow reversal in some parts. In the absence of the impeller blade and due to the pressure difference between the diffuser exit and the diffuser throat, a backflow occurred in the diffuser vane channel, where the highest velocity value was in the throat area, as shown by Wernet et al. [12]. The reversed flow depended on the flow time but spatial variations were also observed. The reversed flow fluid in the diffuser also exhibited stream-wise velocity variation.

(iv) **Recovery flow inception:** This phase started at time interval IV when the flow reattached to the normal direction. The pressure difference that caused the backflow was lower than that observed for the flow reversal shown in Fig. 6. Fig. 7–IV illustrates the start of the flow recovery, which re-established the normal flow direction and pressure recovery through the diffuser, as described by Wernet et al. [12]. Fig. 7–IV shows the velocity field immediately prior to the minimum pressure in the diffuser region. The failure in pressure caused an air movement to flow into the diffuser where the static pressure and mass flow rate increased.

Table 5
Bleeding slot case dimensions.

Slot no.	Bleeding slot position from main blade LE	Bleeding slot and recirculation channel width	Reinjection slot position from main blade LE
1	0.070 D_1	0.019 D_1	0.844 D_1
2	0.147 D_1	0.019 D_1	0.844 D_1
3	0.187 D_1	0.019 D_1	0.844 D_1

(v) **Reattachment phase:** Fig. 7–V shows the continuation of the flow recovery, which was characterized by the highest flow velocity in the diffuser. The maximum velocity detected in this phase was 1.68 U_2. The diffuser flow accelerated when it reached the diffuser throat. A shock wave propagated in front of the low momentum flow region. Clearly, the pressure started to increase to a value close to the stable operating point before the compressor entered another surge cycle.

6. Impeller inducer flow during the surge stages

The unsteady numerical results obtained at the impeller inducer and near the shroud are presented in Fig. 8, where the origin of destabilization generally occurred in this specific location. For the surge flow rate and time "I," the operation under the surge flow led to a gradual decrease in the mean flow velocity, which caused the incidence angle of the main impeller blades to rise. The high incidence at a low mass flow rate and the adverse pressure gradient in the impeller caused the boundary layer to thicken and separate on the impeller's main blade suction side. The tip leakage flow entered the passage upright to the blade suction side. The main impeller flow interacted with the tip leakage flow, which caused a deflection in the tip flow direction. The main flow had a high incidence angle and the tip flow had a different flow angle, so a tip leakage vortex was generated due to the non-uniform flow properties at the impeller inducer. The changes in the axial velocity and the velocity vectors at 95% span of the impeller inducer for different time intervals are presented in Fig. 8. At flow time I, the axial speed was positive at the impeller inlet, but negative axial speed zones were detected at the main blade suction side. In addition, a high positive axial speed region was observed near the pressure side of the main blade.

The inducer area with negative axial velocity was considered as the region into which the tip leakage flow fed, where the region of the tip leakage vortex was bounded by positive and negative axial velocity areas. The main blade tip clearance flow and the boundary layer of the main blade suction side hit the splitter pressure side. Part of this flow moved upstream, thereby creating a reverse flow zone. At flow time II, the zone with negative axial speed extended toward the blade leading edge, inducing large zones with negative axial speed in the impeller passage.

The tip leakage flow from the tip clearance tended to be redirected back toward the impeller inlet, which was caused by the negative pressure gradient. The impeller inlet flow and the reversed flow interacted with each other, which led to the compressor stalling. At flow time III, the reversed flow spread toward the impeller inlet. This back flow originated from the interaction between the main flow and the tip flow, and the diffuser flow also affected the onset of the flow reversal. The reversed flow was observed near the blade tip and close to the shroud. The flow reversal condition was also detected based on the velocity vectors drawn at a span plan near the blade tip.

7. Surge control results

7.1. Effects of the bleeding slot positions on the compressor surge limit

The effects of the bleeding slot positions on the compressor surge limit were determined by changing the bleeding slot positions relative to the main blade's leading edge. The reinjection slot position was kept the same in the three cases. The slot dimensions are shown in Fig. 2 and Table 5. To detect the inception of the surge event, the mass flow at the impeller inlet was monitored during the simulated flow period. Fig. 9 shows the impeller mass flow for the base case and the cases with recirculation slots, where the surge event was detected in the base case and the flow reversal was clearly visible at the impeller inlet. The surge limit increased for the compressor with self-recirculation slots, especially for slot 1 and slot 2. The simulation showed that the bleeding slot positions had a considerable impact on the stable operation of the compressor. Slot position 1 led to the stable operation of the compressor with no flow reversal at the impeller inlet. Slots 2 and 3 had smaller effects on improvements in the surge limit, but high flow fluctuations were detected for slot 2 and the flow was still reversed at the impeller inlet, thereby indicating the presence of surge. Fig. 10 clearly illustrates the effects of the bleeding slot position on the surge limit of the compressor and its overall efficiency.

The efficiency of the compressor at the surge operation point was affected by the bleeding slot positions, where the efficiency decreased to 83.4% for slot 1 and 82.5% for slot 3. The decreased efficiency was caused by increased friction losses in the circulation channel and mixing losses near the reinjection slot. The increases or decreases in the surge limit due to variations in the slot positions can be understood by analyzing the variations in the bleeding flow rate with time, as shown in Fig. 11, where the bleeding flow rate is expressed as a percentage of the operating stage flow rate. As shown in Fig. 11,

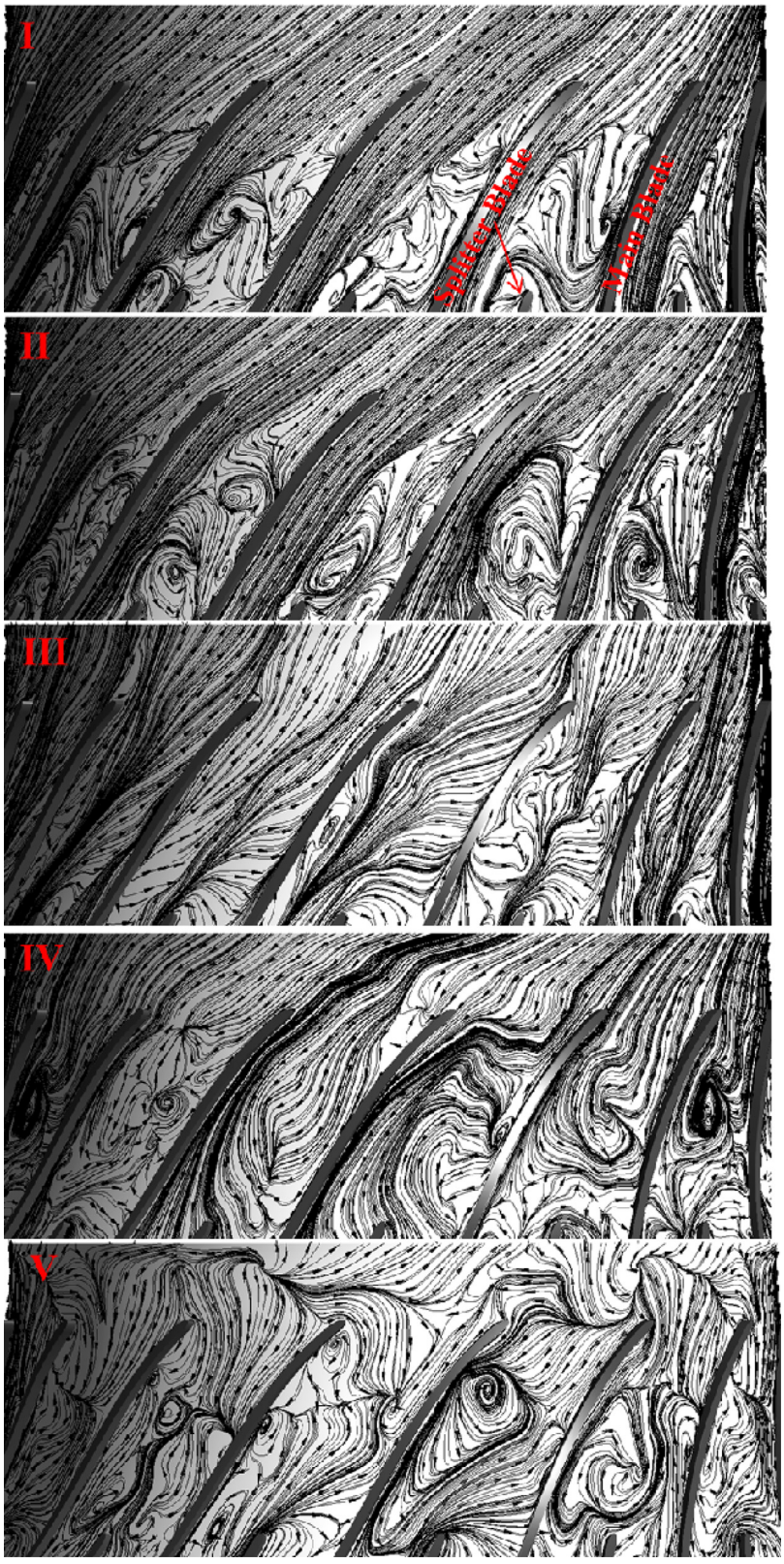

Fig. 8. Streamlines and velocity vectors of the impeller inducer 95% span plane in different surge phases.

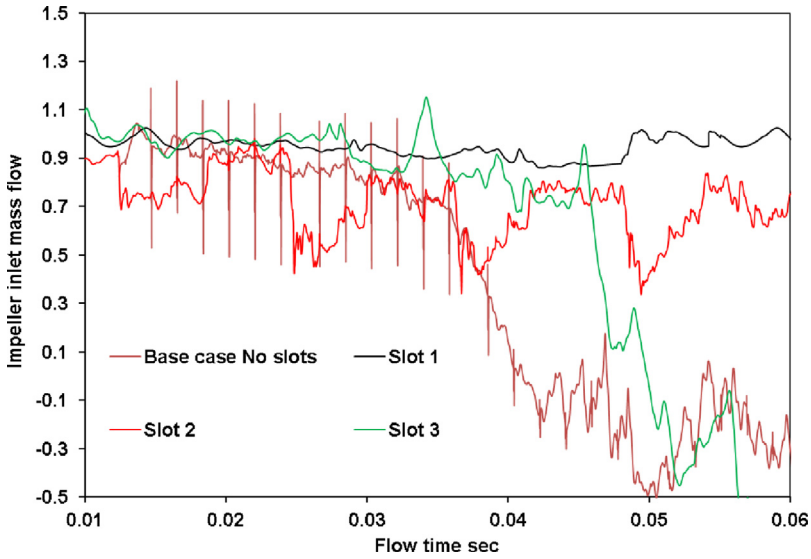

Fig. 9. Dimensionless impeller inlet mass flow caused by the operating mass flow.

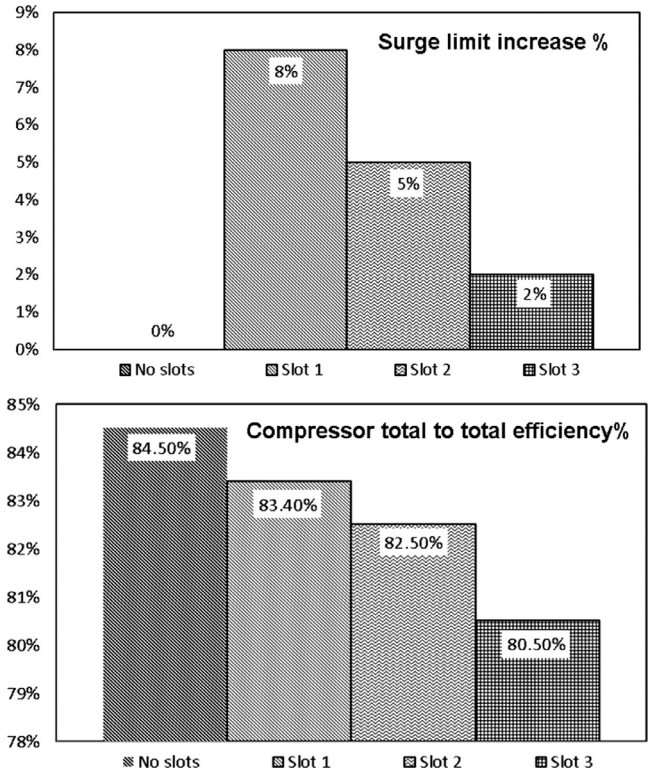

Fig. 10. Effect of the bleeding slots position on the surge limit and compressor efficiency.

the slot 1 obtained a lower flow rate through the recirculation channel than slot 2 or slot 3. Recirculating a larger amount of flow from slot 3 had an adverse effect on the efficiency due to the frictional losses through the slot and mixing losses in the inlet. Fig. 11 shows that the flow recirculated via the rear slot fluctuated with time. The amplitude of the mass flow fluctuation from slot 1 was smaller than that at the rear of slots 2 and 3.

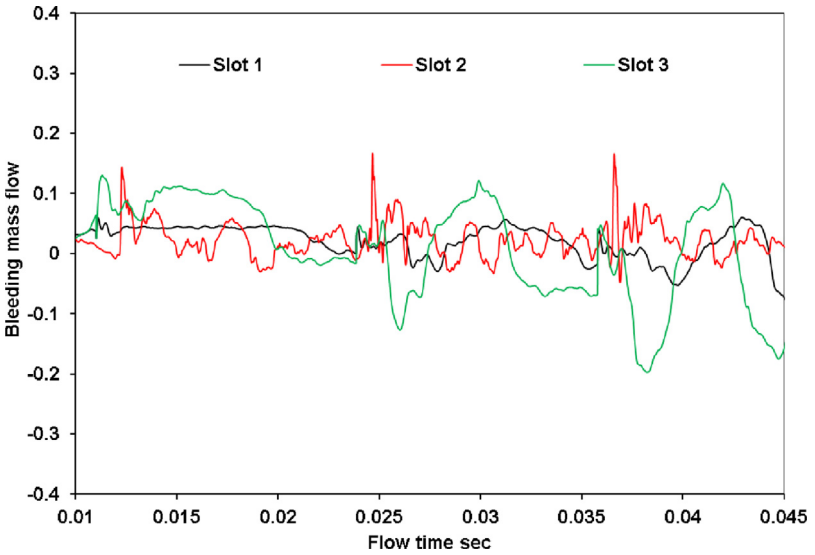

Fig. 11. Dimensionless bleeding mass flow caused by the operating mass flow.

8. Conclusions

In this study, we successfully simulated surge inception and active surge control for a high speed centrifugal compressor. The simulation performed with LES as a turbulence model captured the unsteady large-scale structures and separation zones during the surge event. The results obtained by the LES were compared qualitatively and quantitatively with previously reported experimental data. We determined the static pressure and flow rate, and discussed their changes with the flow time during the surge event. In addition, the impeller flow rate and flow direction were monitored during the flow period and used to specify the surge phases. We investigated active surge control with self-recirculating bleeding slots in three different bleeding slot positions. We analyzed the effects of the slot positions on the surge limit, compressor efficiency, and bleeding mass flow rate. The main results obtained and the phenomena detected can be summarized as follows.

1. The aerodynamic phenomena during the surge event were captured accurately by the LES CFD simulation. Our results also confirmed that LES obtained better predictions of the unsteady flow features in the centrifugal compressor than URANS, especially at lower mass flow rates.
2. An unsteady flow during the surge stages was identified through the diffuser and impeller inducer parts. During surge inception, the rotating instability flow patterns were different for each diffuser channel due to the relative positions of the impeller blades and diffuser vanes. In the reversed flow condition, a non-periodic reversed flow pattern was detected in the diffuser channels as well as through the impeller inducer blade channels. In the flow recovery condition, small stalled cells were observed in front of the shockwave until the flow recovered completely.
3. In the surge flow, the interaction between the recirculating flow and the main inflow stabilized the flow within the impeller inducer, which improved the available flow range. Our analysis determined the effects of the different bleeding slot positions on the surge limit and compressor efficiency. For the nearest slot to the main blade's leading edge, the influence of the recirculating flow increased the surge limit more strongly compared with that for the slots near the split blade's leading edge.
4. The results of the numerical simulation demonstrated that self-recirculating bleeding slots could extend the surge limit of the aero engine centrifugal compressor by about 8% whereas the efficiency decreased by 1%.

Acknowledgment

This study was supported by NPRP grant No. 4-651-2-242 from the Qatar National Research Fund (a member of Qatar Foundation). The statements made herein are solely the responsibility of the authors.

References

[1] T.F. Mckain, G.J. Holbrook, Coordinates for a high performance 4:1 pressure ratio centrifugal compressor, Lewis Research Center, 1997 NASA-23268.
[2] Z.S. Spakovszky, Backward traveling rotating stall waves in centrifugal compressors, J. Turbomach. 126 (2004) 1–12.
[3] G.J. Skoch, P.S. Prahst, M.P. Wernet, A.J. Strazisar, Laser anemometer measurements of the flow field in a 4:1 pressure ratio centrifugal impeller, in: Proceedings of ASME Turbo-Expo 97, Orlando, Florida, 1997.
[4] M.P. Wernet, M.M. Bright, G.J. Skoch, An investigation of surge in a high-speed centrifugal compressor using digital PIV, J. Turbomach. 123 (2002) 418–428.

[5] R.H. Ni, G. Fan, CFD simulation of a high-speed centrifugal compressor using code Leo and code Wand, Aerodynamic Solutions, Inc, 2009 Technical report.
[6] E.A. Lurie, P.R. Van Slooten, G. Medic, J.M. Mulugeta, B.M. Holley, J. Feng, O. Sharma, R.H Ni, Design of a high efficiency compact centrifugal compressor for rotorcraft applications, in: The American Helicopter Society 67th Annual Forum, Virginia Beach, VA, 2011 May 3–5.
[7] K.T. Lim, S.Y. Yoon, C.P. Goyne, Z. Lin, P.E. Allaire, Design and characterization of a centrifugal compressor surge test rig, Int. J. Rotat. Mach. 2011 (June 2011).
[8] Tre'binjac, N. Bulot, N. Buffaz, Analysis of the flow in a transonic centrifugal compressor stage from choke to surge, J. Power Energy 225 (2011) 919.
[9] M. Babak, CFD analysis of a surge suppression device for high pressure ratio centrifugal compressor, in: Proceedings of ANSYS Conference 2010, 2010 Frymburk 6. –8. Října 2010.
[10] J. Galindo, H. Climent, C. Guardiola, A. Tiseira, On the effect of pulsating flow on surge margin of small centrifugal compressors for automotive engines, Exp. Thermal Fluid Sci. 33 (2009) 1163–1171.
[11] N. Bulot, I. Trébinjac, X. Ottavy, P. Kulisa, G. Halter, B. Paoletti, P. Krikorian, Experimental and numerical investigation of the flow field in a high-pressure centrifugal compressor impeller near surge, J. Power Energy 223 (2009) 657.
[12] N. Bulot, I. Trébinjac, Effect of the unsteadiness on the diffuser flow in a transonic centrifugal compressor stage, Int. J. Rotat. Mach. 2009 (June 2009).
[13] G. Arnulfi, F. Blanchini, P. Giannattasio, D. Micheli, P. Pinamonti, Extensive study on the control of centrifugal compressor surge, J. Power Energy 220 (2005) 289.
[14] A. Stein, Computational Analysis of Stall and Separation Control in Centrifugal Compressors, Georgia Institute of Technology, Georgia, 2000 PhD. Thesis.
[15] G. Ferrara, L. Ferrari, L. Baldassarre, Rotating stall in centrifugal compressor vaneless diffuser: experimental analysis of geometrical parameters influence on phenomenon evolution, Int. J. Rotat. Mach. 10 (6) (2004) 433–442.
[16] J. Gravdahla, O. Egelanda, S. Vatlandb, Unsteady Diffuser Flow in a Transonic Centrifugal Compressor, Elsevier Science Ltd, 2002 pii: S 0005-1098(02)00113-9.
[17] S. Sivagnanasundaram, S. Spence, J. Early, Map width enhancement technique for a turbocharger, ASME J. Turbomach. 136 (2014) 061002-1.
[18] K. Beneda, Development of Active Surge Control Devices for Centrifugal Compressors, Budapest University of Technology and Economics, Hungary, June 2013 Ph.D. Thesis.
[19] L. Hu, H. Sun, J. Yi, E. Curtis, J. Zhang, C. Yang, E. Krivitziky, Numerical and experimental investigation of a compressor with active self-recirculation casing treatment for a wide operation range, J. Automob. Eng. (May 2013), doi:10.1177/0954407013486741.
[20] S. Yamaguchi, H. Yamaguchi, S. Goto, F. Nakamura, The development of effective casing treatment for turbocharger compressor, in: Proceedings of the 7th IMechE International Conference on Turbochargers and Turbocharging, London, 2002 May 14–15, Paper No. C602/016/2002.
[21] H. Tamaki, X. Zheng, Y. Zhang, Experimental Investigation of high pressure ratio centrifugal compressor with axisymmetric and nonaxisymmetric recirculation device, ASME J. Turbomach. 135 (2013) 031023-1.
[22] H. Tamaki, Effect of recirculation device with counter swirl vane on performance of high pressure ratio centrifugal compressor, ASME J. Turbomach. 134 (2012) 051036-1.
[23] H. Dickmann, T. Wimmel, J. Szwedowicz, D. Filsinger, D. Roduner, Unsteady flow in a turbocharger centrifugal compressor: three-dimensional computational fluid dynamics simulation and numerical and experimental analysis of impeller blade vibration, ASME J. Turbomach. 128 (2006) 455.
[24] H. Chen, V. Lei, Casing treatment and inlet swirl of centrifugal compressors, ASME J. Turbomach. 135 (2013) 041010-1.
[25] S. Yoon, Z. Lin, W. Jiang, P. Allaire, Flow-rate observers in the suppression of compressor surge using active magnetic bearings, ASME J. Turbomach. 135 (2013) 041015-1.
[26] G. Skoch, Experimental investigation of centrifugal compressor stabilization techniques, ASME J. Turbomach. 125 (2003) 705.
[27] Y. Mingyang, M.B. Ricardo, D. Kangyao, Z. Yangjun, Z. Xinqian, Unsteady influence of self recirculation casing treatment (SRCT) on high pressure ratio centrifugal compressor, Int. J. Heat Fluid Flow 58 (2016) 19–29.
[28] I. Shahin, M. Gadala, M. Alqaradawi, O. Badr, Unsteady CFD simulation for high speed centrifugal compressor operating near surge, in: ASME Turbo Expo 2014: Turbine Technical Conference and Exposition (pp. V02DT44A045-V02DT44A045), American Society of Mechanical Engineers, 2014.
[29] T. Halawa, M. Alqaradawi, M.S. Gadala, I. Shahin, O. Badr, Numerical investigation of rotating stall in centrifugal compressor with vaned and vaneless diffuser, J. Thermal Sci. 24 (4) (2015) 323–333.
[30] I. Shahin, M. Gadala, M. Alqaradawi, O. Badr, Large eddy simulation for a deep surge cycle in a high-speed centrifugal compressor with vaned diffuser, J. Turbomach. 137 (10) (2015) 101007.
[31] ANSYS FLUENT, Theory guide, November 2010.